Enhanced benthic response to upwelling of the Indonesian Throughflow onto the southern shelf of Timor-Leste, Timor Sea

Daniel M. Alongi,[1] Richard Brinkman,[1] Lindsay A. Trott,[1] Fernando da Silva,[2] Francisco Pereira,[2] and Tonny Wagey[3]

Received 15 August 2012; revised 21 November 2012; accepted 1 December 2012.

[1] Benthic microbial metabolism and bacterial diagenetic pathways were measured along the southern shelf of Timor-Leste during an upwelling event in the winter SE monsoon season. Vertical profiles of water properties and bottom water nutrient concentrations, and operational ocean modeling showed subsurface upwelling from the Indonesian Throughflow (ITF) along the southern shelf west of longitude 126°25′E and surface upwelling at the far eastern end of the shelf. Warm surface waters above the halocline had salinities of 33.6 to 33.9 overlying cooler ITF water with salinities of 34.4 to 34.6. Beneath the zone of subsurface upwelling and stratification, sediment chlorophyll *a* (range: 2.8–4.4 $\mu g\, g^{-1}$) and phaeopigment (range: 4.5–7.0 $\mu g\, g^{-1}$) concentrations were sufficient to fuel very rapid rates of benthic oxygen consumption (range: 89.9–142.3 $mmol\, m^{-2}\, day^{-1}$) and dissolved inorganic carbon (DIC) release (range: 108.1–148.9 $mmol\, m^{-2}\, day^{-1}$) across the sediment-water interface, and DIC (range: 94.7–142.5 $mmol\, m^{-2}\, day^{-1}$) and NH_4^+ (range: 13.3–19.9 $mmol\, m^{-2}\, day^{-1}$) production from incubated surface (0–10 cm) sediments. Molar ratios of DIC/NH_4^+ production were lower (range: 6.6–7.7) in fine-grained sediments under the subsurface upwelling regime than in sandy, possibly scoured sediments under surface upwelling (range: 11.9–21.2) where there was no evidence of benthic enrichment. It is proposed that subsurface upwelling along the widest portions of the shelf stimulates phytoplankton production, leading to deposition of fresh phytodetritus that is rapidly decomposed on the seafloor. These zones of high biological activity may attract and support large populations of pelagic fish and cetaceans that have been caught for centuries along the south coast.

Citation: Alongi, D. M., R. Brinkman, L. A. Trott, F. da Silva, F. Pereira and T. Wagey (2013), Enhanced benthic response to upwelling of the Indonesian Throughflow onto the southern shelf of Timor-Leste, Timor Sea, *J. Geophys. Res. Biogeosci.*, *118*, doi:10.1029/2012JG002150.

1. Introduction

[2] The Timor Sea is an important oceanographic conduit linking the Pacific and Indian oceans. The main water mass linking both oceans is the Indonesian Throughflow (ITF), part of which transits through the Timor Sea. The ITF transports roughly 15 Sv from the Pacific to the Indian Ocean, forming the warm-water route for the global thermohaline circulation and providing a path for water to circumnavigate the global ocean [*Gordon and Fine*, 1996; *Sprintall*, 2009; *Tillinger*, 2011]. The ITF is thus closely linked to global climate via the El Niño/Southern Oscillation phenomenon and the Indian Ocean Dipole [*Saji et al.*, 1999; *England and Huang*, 2005]. Due primarily to a pressure gradient induced by differences in sea level between the Pacific and Indian oceans, water from the North Pacific enters the Sulawesi Sea and continues through the Makassar Strait and, to a lesser extent, the Lifamatola Passage. The ITF then exits via Lombok Strait or circulates through the Banda and Flores seas and enters the Indian Ocean via Ombai Strait and Timor Passage [*Atmadipoera et al.*, 2009]. Recent estimates indicate that roughly half of ITF water outflows through the Timor Passage [*Tillinger*, 2011]. This relatively low-salinity water flows south of the island of Timor in a westerly direction within the upper 200 m at speeds up to 0.5 $m\, s^{-1}$ with a weak secondary flow near 1200 m depth [*Molcard et al.*, 1996]. The Timor Sea is under the influence of the NW monsoon from November to March when surface flow is northeasterly, and from May to September when the SE monsoon prevails, with surface flow reverting to the west from March to August [*Cresswell et al.*, 1993; *Schiller et al.*, 2010].

[3] Variations in the strength of the ITF have been linked inversely to variations in paleoproductivity in the Timor Sea [*Müller and Opdyke*, 2000; *Holbourn et al.*, 2005; *Xu et al.*, 2006]. Although coastal upwelling occurs at the edge of the northern Australian shelf [*Furnas*, 2007; *McKinnon*

[1]Australian Institute of Marine Science, Townsville, Queensland, Australia.
[2]Departamento de Geslav de Recursos Pesqueiros, Ministeris de Agricultura, Florestas e Pescas, Comoro, Dili, Timor Leste.
[3]Arafura and Timor Seas Ecosystem Action, Agency for Marine and Fisheries Research Jalan Mt. Haryono Kav, Jakarta, Indonesia.

Corresponding author: Daniel M. Alongi, Australian Institute of Marine Science, PMB 3, Townsville MC, Queensland 4810, Australia. (d.alongi@aims.gov.au)

2169-8953/13/2012JG002150

et al., 2011] and in the eastern Banda and northern Arafura seas [*Gieskes et al*., 1990], it is not known what effect, if any, the ITF has on productivity in the northern Timor Sea in close proximity of the island of Timor. The region is ecologically and physically diverse, yet little scientific information is available. The narrow southern shelf of Timor was once sampled extensively in 1900 by the Siboga Expedition [*Weber*, 1902], which identified areas of fine sediment along most of the Timorese coast, with coarser sand and coral deposits east of longitude 127°.

[4] To address the paucity of information and as part of a larger project on the Timor and Arafura seas (http://atsea-program.org), we conducted a benthic survey along the south coast of Timor-Leste during the SE monsoon season to measure rates and pathways of sediment metabolism in relation to sediment grain size, nutrient concentrations, and the origin of sedimentary organic matter. As detailed here, we found very rapid rates of metabolism along sections of the shelf edge that appear to be in response to upwelling of water from the ITF.

2. Methods

2.1. Study Site and Field Sampling

[5] The continental shelf of southern Timor-Leste (Figure 1) is a narrow, active margin that is part of the Banda Arc where isostatic rebound of previously subducted Australian crust has resulted in regional uplift [*Harris*, 1991; *Richardson and Blundell*, 1996]. This portion of the Banda Arc is a nonvolcanic collision zone, but uplift is active today as evidenced by the widespread occurrence of raised Pliocene to Holocene coral reef terraces hundreds of meters thick along the coast [*Chappell and Veeh*, 1978].

[6] Timor-Leste experiences a dry season from July to October and a wet season from November to March with an average annual rainfall of 1500 to 2000 mm along the mountainous spine of the island and along the southern coast [*Durand*, 2002]. The south coast contains more than 20 small rivers that drain rapidly eroding, short, steep catchments. Rapid uplift, heavy rainfall, rapid weathering, and extensive deforestation result in an average sediment load of 60 Mt yr^{-1} [*Milliman et al*., 1999]. The narrow shelf (defined here as the ≤300 m contour) along the south coast is 11 km wide at its widest point near Suai, but shelf width is ≤2 km at several capes along the coast. Total shelf area is approximately 1580 km^2 along a coastline length of 285 km for an average shelf width of about 5.5 km.

[7] Twenty stations were visited from 10 to 18 July 2011 on the RV *Solander*. These stations covered the entire length of the south coast (Figure 1). At each station, conductivity-temperature-depth (CTD) and Niskin casts were taken for measurement of water-column structure and bottom water nutrients, and benthic grab or boxcorer samples were taken for measurements of sediment characteristics and microbial metabolism.

2.2. Water-Column Measurements and Oceanic Modeling

[8] CTD casts at each station were made using a Seabird SBE911Plus Livewire CTD (Sea-Bird Electronics, Inc., Bellevue, Wash.) fitted with a LICOR Photosynthetically Active Radiation (PAR) sensor (LICOR, Lincoln, Nebr.), a Seabird SBE43 oxygen sensor, and a Chelsea chlorophyll fluorometer (Chelsea Technologies, West Molesey, Surrey, UK). A separate cast was taken using a 10-L Niskin bottle to obtain water samples for measurement of water-column nutrients 1 m above the seafloor. Water samples were collected from Niskin bottles using acid-washed syringes and filtered through a 0.45 µm filter cartridge (Sartorius Minisart) into acid-washed screw-cap plastic test tubes and stored frozen (−18°C) until later analysis ashore. DOC samples were acidified with 100 µl analytical reagent-grade

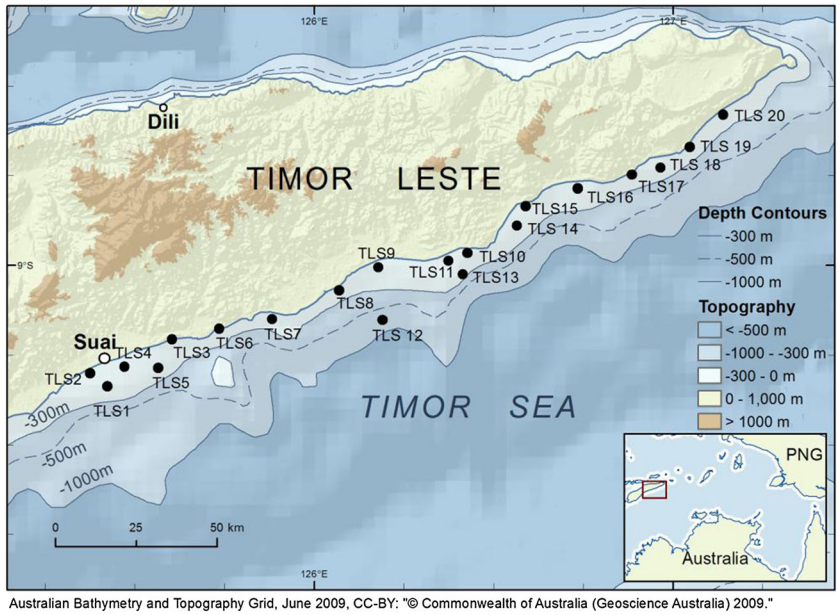

Figure 1. Chart of the 20 benthic stations along the southern shelf of Timor-Leste sampled during July 2011. © Commonwealth of Australia (Geoscience Australia), 2009.

HCl and stored at 4°C until analysis. Inorganic dissolved nutrient concentrations were determined by standard wet chemical methods [*Ryle et al*., 1981] implemented on a segmented flow analyzer [*Bran and Luebbe*, 1997].

[9] Thicknesses of the mixed layer, the isothermal layer, and the top of the thermocline were estimated using the gradient analysis criteria of *Lucas and Lindstrom* [1991]. A 5 m starting depth was used to avoid misclassifications due to near-surface disturbance. A density gradient of 0.01 kg m^{-1} was used to determine the mixed-layer depth. To determine the thickness of the isothermal layer and the top of the thermocline, we used critical temperature gradients of 0.025°C m^{-1} and 0.05°C m^{-1}. CTD profiles at each station were searched downward until each of the criteria was met between at least three consecutive 1 m depths. Layer depth was assigned the shallowest value.

[10] Three-dimensional descriptions of potential temperature during the period of this study were obtained from the Australian Bureau of Meteorology OceanMAPS forecasting system, based on an operational implementation of the Ocean Forecast Australia Model (OFAM) [*Schiller et al*., 2008]. OFAM is based on version 4.0 of the Modular Ocean Model [*Griffies et al*., 2004], with a resolution grading from 2° in the North Atlantic to 1/10° in the Asian–Australian region from 90°E to 180°E and from 16°N to 75°S. The model grid contains 47 levels in the vertical, 35 of which are in the top 1000 m, with 10 m resolution near the surface. The model uses hybrid mixed-layer representation; horizontal viscosity is resolution and state dependent based on the Smagorinsky scheme, and due to the model's variable grid size, anisotropic options have been chosen for this parameterization [*Schiller et al*., 2008]. The performance of the OFAM model in the region covering the shelf of southern Timor-Leste has been evaluated against observations of potential temperature and velocity from moorings within the straits of Timor and Ombai, and the model agrees reasonably well with these observations [*Schiller et al*., 2010].

2.3. Bulk Sediment Measurements

[11] Sediment samples were taken from a 0.2 m^2 Smith-McIntyre grab with rubber-sealed lids. Samples were taken only from sediments having intact surface sediment structures such as animal tracks, tubes, and burrow openings. Surface (0–5 cm) samples were taken for measurement of total carbon (TC), total organic carbon (TOC), and total nitrogen (TN) content and for measurement of $^{13}\delta$C and $^{15}\delta$N content and for chlorophyll a and phaeopigments. A large sample (>100 g) was also taken for sediment granulometry. Grain size was determined on an automated particle size counter and sediment type classified based on the definitions in *Folk* (1974). Samples for TC, TOC, and TN were frozen, wet-weighted, and dry-weighted to determine water content and porosity before and after freeze-drying and ground to a fine powder for determination of TC and TN on a Perkin-Elmer 2400 CHNS/O Series II Analyzer (Perkin-Elmer, Waltham, MA, USA) and for TOC on a Shimadzu TOC Analyzer with solid sampler (Shimadzu Corp., Tokyo, Japan). Analytical performance was monitored with standard reference materials NBS 1646 (estuarine sediment) from National Institute of Standards Technology and BCSS-1 (marine sediment) obtained from the National Research Council of Canada. Values were always within the certified range. Detection limits for solid-phase metals were 5 μg g^{-1} sediment dry weight on the Thermo IRIS AAS. Total inorganic carbon was assumed as $CaCO_3$ and was determined by difference between the TC and TOC concentrations.

[12] Samples for benthic pigments were taken from surface (0–2 cm) sediments using a 5 ml syringe with the needle end cut off. Chlorophyll *a* and phaeopigments were extracted using a 1:1 (v/v) chloroform-methanol solution [*Wood*, 1985]. Absorbance was measured at 665 nm on a Varian spectrometer. The spectrophotometric equations of *Lorenzen* [1967] were modified to account for the use of a different extractant.

[13] Samples for stable isotopes were collected using rubber gloves and a clean metal spatula to avoid contamination. Samples were placed in clean glass vials and frozen until return to the lab. Samples were then freeze-dried and stored in airtight desiccators with silica gel. Subsamples (1 g) were transferred to 15 ml centrifuge tubes and 7 ml cold 10% HCl was added, 0.5 ml at a time to avoid overflow. Samples were left to react overnight; drops of cold acid were then added if necessary to complete the dissolution of carbonate. Once completely acidified, samples were washed with cold distilled water twice and oven-dried (60°C for 1–2 days). Samples were left in desiccators until analysis. Each sample was weighed and packed tightly in individual tin SerCon capsules (5 mm width, 8 mm height) and compressed, ensuring no air was left in the capsules. Samples were analyzed for N and C content (%), δ^{15}N, and δ^{13}C using an Automated Nitrogen Carbon Analyzer-Mass Spectrometer consisting of a 20/20 mass spectrometer connected with an ANCA-S1 preparation system (Europa Scientific Ltd., Crewe, UK). Results were normalized according to *Paul et al*. [2007].

[14] A simple two end-member mixing equation [*Tyson*, 1997, p. 396] was used to estimate the fraction of δ^{13}C derived from terrestrial and marine sources. The terrestrial (−27‰) and marine (−19‰) end-members of *Aller et al*., [2008] from the Gulf of Papua were used.

2.4. Fluxes Across the Sediment-Water Interface

[15] Solute fluxes across the sediment-water interface at each station were measured using three to six opaque chambers (volume: 1 L; area: 82 cm^2; height: 20.5 cm) from which DIC samples were taken at 1 h intervals for 4–6 h. Each chamber was gently placed into the surface sediment of minimally disturbed grab samples. Each chamber was then withdrawn after a fitted plastic bottom lined with soft rubber was placed and fit to the chamber bottom by hand. The outside of each chamber was washed, and the entire set of chambers was then incubated under shade in a running seawater bath to maintain in situ seawater temperature. Each chamber had a propeller-electric motor unit placed within the top opening of the chamber. Three sampling ports were located on opposite sides of the chamber: (1) one port was fitted with tubing that opened to allow replacement water to enter [*Alongi et al*., 2007]; (2) the second port was fitted with an O_2 probe (TPS Model WP-82 DO meters) to measure dissolved oxygen flux; and (3) the third port was fitted with plastic tubing to draw off 10-ml samples for DIC and dissolved inorganic nutrients (DIN). Samples were filtered (0.45 μm Minisart filters) and kept cool and dark for DIC, and frozen for DIN. Concentrations of DIC were determined

using the procedure of *Hall and Aller* [1992], and DIN concentrations were determined as described in section 2.2.

2.5. Incubation Experiments: DIC and NH_4^+ Production and Metal Reduction in Sediments

[16] Rates of net release of dissolved Fe, Mn, DIC, and NH_4^+ from sediments at each site were measured by using a sediment incubation technique [*Alongi et al.*, 2007]. At each station, sediment slices were taken over the 0–10 cm depth interval by sinking opaque glass jars into the sediment. Further sediment was added so no airspace was present; then each jar was capped and sealed with electrical tape. The jars where then incubated at in situ temperature for 6–12 d. At the end of each incubation, 30–40 ml homogenized sediment

Table 1. Mean Water-Column Characteristics From CTD Casts Taken at Each of the Stations Along the South Timorese Coast[a]

Station	Latitude (S)	Longitude (E)	1% PAR (m)	WD (m)	MLD (m)	ITL (m)	TT (m)	SST/SBT (°C)	SSS/SBS	SSDO/SBDO (mg L^{-1})
TLS1	9°20.172’	125°25.36’	27	133	39	39	42	26.59/20.18	33.68/34.55	6.62/7.37
TLS2	9°17.971’	125°22.52’	24	52	10	10	31	26.57/24.40	33.73/34.34	6.62/6.84
TLS3	9°12.335’	125°36.20’	7	50	19	19	19	26.34/24.71	33.79/34.33	6.65/6.81
TLS4	9°16.880’	125°28.26’	21	81	9	6	9	26.58/22.98	33.74/34.45	6.62/7.02
TLS5	9°17.143’	125°33.88’	5	157	37	36	38	26.49/16.17	33.72/34.59	6.63/7.96
TLS6	9°10.493’	125°44.09’	19	144	10	10	10	26.46/16.12	33.73/34.56	6.63/8.25
TLS7	9°08.947’	125°52.91’	10	88	11	11	11	26.10/23.56	33.86/34.42	6.67/6.95
TLS8	9°04.172’	126°04.11’	14	105	6	6	9	26.46/20.63	33.66/34.53	6.64/7.32
TLS9	9°00.288’	126°10.74’	15	60	33	32	33	26.20/24.72	33.76/34.27	6.66/6.82
TLS10	8°57.908’	125°25.61’	20	148	10	6	35	26.45/15.66	33.71/34.56	6.64/8.04
TLS11	8°59.201’	126°22.44’	9	39	9	8	9	26.45/24.91	33.77/34.26	6.63/6.79
TLS13	9°01.496’	126°24.82’	23	120	15	14	16	26.78/18.56	33.73/34.45	6.60/7.60
TLS14	8°53.338’	126°33.91’	2	94	30	29	30	26.77/22.21	33.77/33.46	6.60/7.11
TLS15	8°50.048’	126°35.30’	5	32	30	27	28	26.46/26.14	33.60/33.86	6.64/6.67
TLS16	8°47.063’	126°44.07’	13	39	32	17	28	26.45/26.31	33.81/33.88	6.63/6.64
TLS17	8°44.790’	126°53.09’	17	62	62	—	—	26.44/26.32	33.81/33.89	6.64/6.64
TLS18	8°43.626’	126°57.92’	17	93	61	36	37	26.36/24.11	33.92/34.39	6.64/6.88
TLS19	8°40.126’	127°02.74’	14	70	70	—	—	26.40/23.25	33.87/34.46	6.63/6.98
TLS20	8°34.692’	127°08.38’	12	31	31	—	—	26.27/25.16	33.72/34.11	6.66/6.77

[a]ITL, thickness of isothermal layer; MLD, mixed layer depth; 1% PAR, depth of 1% incident light; SBDO, sea bottom dissolved oxygen; SBS, sea bottom salinity; SBT, sea bottom temperature; SSDO, sea surface dissolved oxygen; SSS, sea surface salinity; SST, sea surface temperature; TT, top of thermocline; WD, water depth.

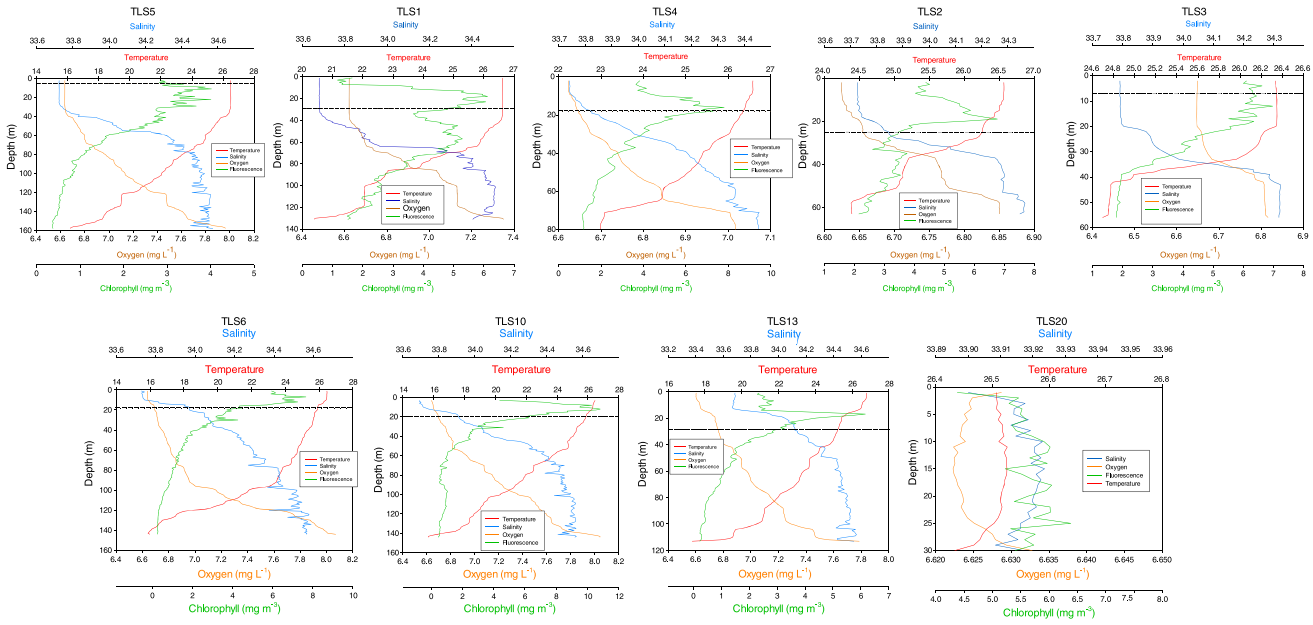

Figure 2. Vertical structure of water properties and the 1% light level (horizontal line in each panel) across the widest section of the shelf (top row, from shelf-edge Sta. TLS5 to inshore Sta. TLS3), upwelling at the narrowest section (Sta. TLS6, bottom left) and further east (Stas. TLS10 and TLS13, bottom middle panels) along the shelf. East of longitude 126°25’, inshore waters were well mixed (e.g., Sta. TLS20, bottom right).

from each jar was placed into a 50 ml centrifuge tube and centrifuged, after which the supernatant was filtered for DIC, SO_4, NH_4^+, Ca, Mg, and Cl analysis. A 1 N KCl solution was then added to each centrifuge tube, mixed into each sample, and after 2–3 h incubation centrifuged again to obtain total extractable NH_4^+, which was determined using automated techniques described in section 2.2.

[17] To obtain preincubation concentrations of all solutes, another set of sediment samples from the same five to eight depth intervals was taken concurrently and centrifuged immediately to obtain pore water as described earlier. Each incubated jar sample was used for determination of both DIC and NH_4^+ reaction rates. DIC was processed as described in section 2.4.

[18] For Fe and Mn reduction, two different sets of jar samples were processed as described earlier. Pore water SO_4^{2-} concentration in jar sediments was increased by 10 mmol L^{-1} to avoid depletion during incubation and mixed thoroughly under a constant N_2 stream. The homogeneous sediment mixtures from each depth interval were transferred into eight 20 ml glass scintillation vials, which were capped with no headspace, taped to prevent oxygen intrusion, and incubated in the dark as close as possible to in situ temperature. Two vials were sacrificed at 6 to 12 day intervals for determination of pore water Fe^{2+} concentrations. Pore water was extracted from the jars by centrifuging at 2500 rpm for 15 min, returned to the glove bag, and filtered through Whatman GF/F filters. Samples were then acidified (20 µl of 0.5 mol L^{-1} HCl per 1 ml) and stored at 5°C in polyethylene vials until analysis by the spectrophotometric ferrozine technique [*Stookey*, 1970], in which a 50 µl sample is transferred to 2 ml of 0.02% ferrozine in 50 mmol L^{-1} 4-(2-hydroxyethyl)-1-piperazine ethanesulfonic acid buffer, pH 7.

[19] The sediment remaining after pore water extraction was homogenized under N_2 for reactive Fe(II) extraction by a modified version of the HCl technique of *Lovley and Phillips* [1987]. In brief, 100–300 mg subsamples were extracted in 5 ml of 0.5 mol L^{-1} HCl for 15 min on a shaking platform at 25°C and centrifuged (5000 rpm for 10 min). The supernatant was GF/F filtered and stored at 5°C until analysis as described earlier for Fe^{2+}. Total dissolved Mn in both extracts was analyzed on the inductively coupled plasma-atomic absorption spectrometer. It was not possible to determine Mn oxidation state due to interference from extractable Fe^{2+}.

[20] Reaction rates were calculated from a linear fit of concentration changes in the time series of samples. Metal reduction rates (corrected for compaction during pore water extraction) were determined as reactive Fe(II) and Mn accumulation assuming limited precipitation into nonacid extractable phases [*Canfield et al.*, 1993]. Reactive amorphous oxyhydroxide concentrations were operationally defined as the difference between total Fe and Mn content measured from acidified samples on the ICP-AES.

2.6. Sulfate Reduction

[21] Sulfate reduction was measured separately in triplicate 2.7 cm diameter plastic cores taken from surface to bottom of each grab sample to a maximum depth of 20 cm. Cores were injected at 1 cm intervals with carrier-free ^{35}S [*Fossing and Jorgensen*, 1989], incubated in time series at 20 min and at 1 h, 3 h, 6 h, and 9 h at stations (Stas.) TLS1, TLS4 and TLS20, and for 6–9 h at the other stations. Incubations were terminated by immediately fixing sediments in 20% zinc acetate. Samples were then frozen until a two-step distillation procedure was used to determine the fraction of reduced radiolabel shunted into the acid-volatile sulfide and chromium-reducible sulfur pools.

3. Results

3.1. Water-Column Structure and Nutrients

[22] Timor shelf stations were between 32 and 157 m in depth and, except for Stas. TLS17, TLS19, and TLS20, the water-column was stratified with the mixed-layer depth varying from 6 to 70 m (Table 1). Except for Stas. TLS2,

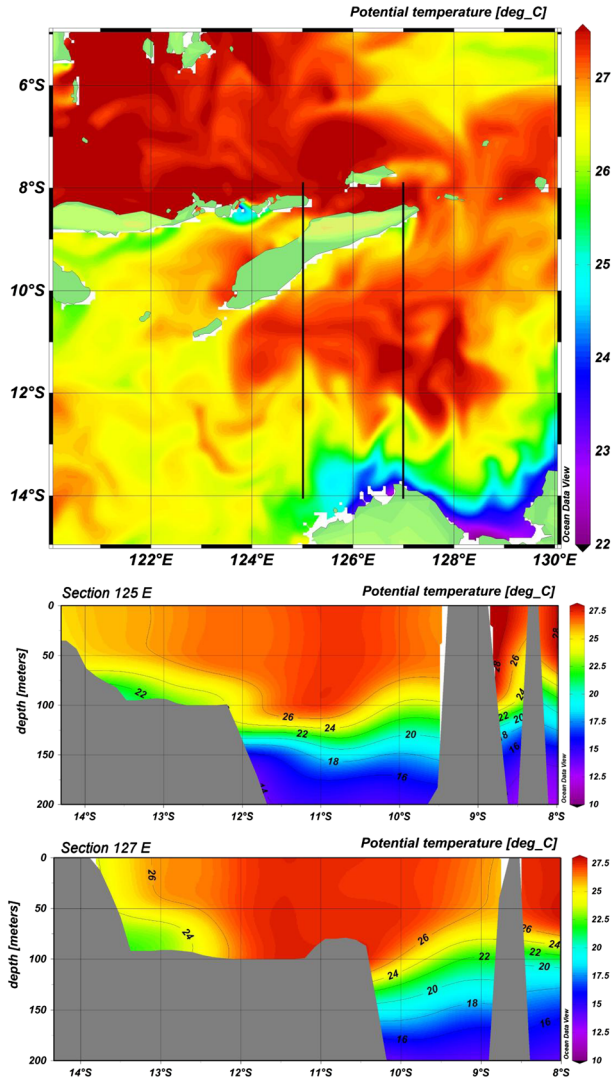

Figure 3. Synoptic view of surface temperature from OceanMAPS model on 17 July 2011 (top) with vertical sections of potential temperature along the longitude 125° (middle) and 127° (bottom) meridians, showing only surface 200 m. Thick lines in top panel show locations of meridional sections. Note change in color scaling between synoptic and sections plots.

TLS10, and TLS18, estimated depth of the mixed layer was shallower and within a few meters of the estimates of the isothermal layer and the top of the thermocline (Table 1) and, at most stations, shallower than the top of the halocline. Surface layers were well mixed at most stations with high turbidity, resulting in the 1% isolume occurring as shallow as less than 10 m at Stas. TLS3, TLS5, TLS7, TLS11, TLS14, and TLS15 (Table 1).

[23] Across the widest section of the shelf (Figure 2, top, from left to right), subsurface intrusions of cool (<20.2°C), nutrient-rich water were evident at Stas. TLS5, TLS4, and TLS1; further landward, the shelf was still stratified within 2 km from small river catchments (Stas. TLS2 and TLS3), but bottom temperatures were warm (>24°C) and dissolved nutrient concentrations low. Vertical structure of water properties indicated upwelling at a very narrow section of the shelf (Sta. TLS6, Figure 2, bottom left), as well as along another wide section of the shelf edge further east (Stas. TLS10 and TLS13, Figure 2, bottom two middle panels). At most of the upwelling stations, there was a well-defined chlorophyll maximum just above the 1% light level (e.g., Stas. TLS1, TLS4, TLS6, TLS10, TLS13, Figure 2). As noted earlier, waters were well mixed at Stas. TLS17, TLS19, and TLS20 (Figure 2, bottom right).

[24] Surface and subsurface intrusions of ITF water onto the southern Timorese shelf was confirmed by a synoptic view of surface temperature (Figure 3, top) on 17 July 2011 from the OceanMAPS model. The 127°E meridional section (Figure 3, bottom) shows a persistent surface signature of upwelling along the eastern end of the southern coast, whereas the 125°E meridional section (Figure 3, middle) confirms subsurface intrusions beneath warm surface waters.

[25] Bottom water phosphate ($r = +0.887$), nitrate ($r = +0.899$), and silicate ($r = +0.902$) concentrations correlated positively ($P < 0.0001$) with water depth (Figure 4).

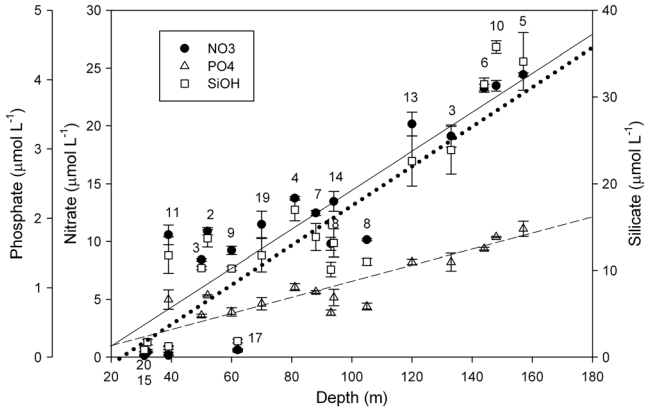

Figure 4. Bottom water concentrations (µmol L^{-1}) of nitrate, phosphate, and silicate in relation to water depth along southern Timor-Leste. Station numbers are listed above each set of values for a given water depth. Error bars are ± 1 standard deviation. All regressions are significant ($P < 0.001$). Nitrate (solid line) = $-2.786 + 0.172x$, $R^2 = 0.809$, $F_{1,18} = 71.866$; phosphate (dashed line) = $-0.142 + 0.0118x$, $R^2 = 0.786$, $F_{1,18} = 62.428$; silicate (dotted line) = $-5.193 + 0.235x$, $R^2 = 0.813$, $F_{1,18} = 73.765$.

Table 2. Mean Sediment Granulometry and Composition, TOC and TN Concentrations, Stable Isotope Values, Percentages of Terrestrially Derived Organic Carbon, and Surface Benthic Chlorophyll *a* and Phaeopigment Concentrations at Stations Along the South Timorese Coast (values are mean ± 1 standard deviation)[a]

Station	Grain Size (µm)	Silt (% WW)	Clay (% WW)	Sand (% WW)	TOC (% sed DW)	TN (% sed DW)	$\delta^{15}N$ (‰)	$\delta^{13}C_{ORG}$ (‰)	OC_{TERR} (%)	Chlorophyll *a* (µg g^{-1})	Phaeopigment (µg g^{-1})
TLS1	7.6 (vfs)	71.7	23.5	4.8	0.65 ± 0.02	0.05 ± 0.01	2.86 ± 0.25	−24.38 ± 0.10	48	2.8 ± 0.3	4.5 ± 1.0
TLS2	7.6 (vfs)	73.6	22.1	4.3	0.50 ± 0.07	0.04 ± 0.01	2.64 ± 0.18	−24.38 ± 0.04	48	0.8 ± 0.6	0.2 ± 0.0
TLS3	8.4 (fs)	73.0	21.9	5.1	0.65 ± 0.02	0.05 ± 0.01	2.83 ± 0.42	−23.97 ± 0.09	43	0.5 ± 0.3	0.1 ± 0.1
TLS4	16.3 (ms)	74.5	23.2	2.3	0.60 ± 0.01	0.05 ± 0.01	2.68 ± 0.19	−24.64 ± 0.08	51	1.0 ± 0.5	2.2 ± 0.7
TLS5	64.9 (vfsd)	40.3	8.9	50.8	0.49 ± 0.01	0.04 ± 0.01	3.18 ± 0.24	−23.61 ± 0.12	38	4.4 ± 0.2	5.5 ± 1.5
TLS6	7.7 (vfs)	72.2	26.7	1.1	0.72 ± 0.07	0.06 ± 0.01	2.66 ± 0.33	−24.64 ± 0.24	51	4.0 ± 0.3	6.4 ± 2.3
TLS7	14.5 (fs)	74.0	22.0	4.0	0.63 ± 0.03	0.05 ± 0.01	2.76 ± 0.18	−23.74 ± 0.15	40	0.8 ± 0.6	1.4 ± 1.1
TLS8	17.2 (ms)	74.1	17.4	8.5	0.56 ± 0.04	0.03 ± 0.0	2.20 ± 0.21	−25.48 ± 0.49	62	0.4 ± 0.2	0.0 ± 0.0
TLS9	7.7 (vfs)	73.4	26.4	0.2	0.75 ± 0.06	0.05 ± 0.0	2.67 ± 0.24	−24.61 ± 0.18	51	0.3 ± 0.2	0.0 ± 0.0
TLS10	83.7 (vfsd)	36.5	9.1	54.4	0.69 ± 0.03	0.06 ± 0.01	3.51 ± 0.48	−22.44 ± 0.07	24	2.9 ± 0.2	7.0 ± 2.2
TLS11	10.1 (fs)	77.6	18.4	4.0	0.78 ± 0.02	0.06 ± 0.01	2.87 ± 0.91	−23.56 ± 0.11	38	0.6 ± 0.3	0.3 ± 0.1
TLS13	431.8 (msd)	19.2	6.2	74.6	0.28 ± 0.01	0.03 ± 0.0	4.13 ± 0.30	−22.27 ± 0.06	22	3.1 ± 0.3	6.5 ± 1.9
TLS14	9.9 (fs)	79.9	18.2	1.9	0.77 ± 0.04	0.07 ± 0.01	3.11 ± 0.43	−23.65 ± 0.22	39	0.7 ± 0.3	0.3 ± 0.1
TLS15	9.8 (fs)	74.4	17.3	8.3	0.83 ± 0.05	0.07 ± 0.01	2.25 ± 0.42	−25.14 ± 0.06	57	0.0 ± 0.0	0.0 ± 0.0
TLS16	14.3 (fs)	74.2	17.9	7.9	0.73 ± 0.03	0.06 ± 0.02	2.43 ± 0.11	−25.67 ± 0.26	64	0.1 ± 0.1	0.0 ± 0.0
TLS17	38.7 (cs)	75.1	13.4	11.5	0.80 ± 0.04	0.07 ± 0.01	2.42 ± 0.27	−25.52 ± 0.16	62	0.1 ± 0.1	0.0 ± 0.0
TLS18	14.4 (fs)	70.1	21.0	8.9	0.60 ± 0.01	0.06 ± 0.01	2.72 ± 0.56	−24.74 ± 0.16	52	0.3 ± 0.1	0.0 ± 0.0
TLS19	158.9 (fsd)	42.7	8.8	48.5	0.53 ± 0.02	0.06 ± 0.01	2.51 ± 0.91	−24.38 ± 0.31	48	0.4 ± 0.1	0.0 ± 0.0
TLS20	109.6 (vfsd)	45.6	7.3	47.1	2.00 ± 0.66	0.10 ± 0.01	1.62 ± 0.16	−28.65 ± 0.31	100	0.0 ± 0.0	0.0 ± 0.0

[a] cs, coarse silt; DW, dry weight; fs, fine silt; fsd, fine sand; ms, medium silt; msd, medium sand; vfs, very fine silt; vfsd, very fine sand; WW, wet weight.

3.2. Sediment Granulometry, Nutrients, and Plant Pigments

[26] Surface sediments at Stas. TLS5, TLS10, TLS13, TLS19, and TLS20 were composed of very fine to medium quartz sand; the remaining stations were composed of very fine to coarse silt, with amounts of clay ranging from 13.4% to 26.7% sediment wet weight (Table 2). Concentrations of TOC and TN along the shelf ranged from 0.28% to 2.0% and from 0.03% to 0.10%, respectively (Table 2), with highest values recorded at Sta. TLS20 where large amounts of plant detritus were found. Both TOC and TN correlated inversely, but weakly (both $r = -0.435$; $P < 0.0626$), with water depth.

[27] Sediment $\delta\ ^{13}C_{ORG}$ and $\delta\ ^{15}N$ values ranged from -28.65 to -22.44 and from 1.62 to 4.13, respectively, and correlated with water depth ($r = +0.523$, $P < 0.0215$; and $r = +0.593$, $P < 0.00749$, respectively). Lowest stable isotope values were recorded at Sta. TLS20. The percentage of sediment organic carbon of terrestrial origin varied from 24% to 100% (Table 2), with highest percentages recorded closest to the coast, as reflected in the inverse correlation with water depth ($r = -0.527$; $P < 0.0205$). Molar C:N ratios varied from 6.6 to 21.2, with the highest ratio recorded at Sta. TLS20; C:N ratios did not correlate significantly ($P > 0.05$) with water depth ($r = +0.0669$).

[28] Chlorophyll *a* and phaeopigment concentrations at the sediment surface (Table 2) varied from 0.0 to 4.0 $\mu g\ g^{-1}$ and from 0.0 to 7.0 $\mu g\ g^{-1}$ sediment dry weight, respectively. Both chlorophyll *a* ($r = +0.873$; $P < 0.0001$) and phaeopigment ($r = +0.841$; $P < 0.0001$) concentrations correlated linearly with water depth (Figure 5).

3.3.. Surface Sediment Metabolism

[29] Rates of oxygen consumption (Figure 6) ranged from 29.6 to 142.3 mmol m^{-2} day^{-1}, and rates of DIC release (Figure 7) ranged from 30.7 to 148.9 mmol m^{-2} day^{-1} among stations. Rates of both O_2 uptake and DIC metabolism in surface sediments related best to surface concentrations of chlorophyll *a* + phaeopigment. Linear regression coefficients of plant pigments with O_2 and DIC metabolism were $r = +0.939$ and $r = +0.921$, respectively, with highest metabolic rates at Stas. TLS1, TLS5, TLS6, TLS10, and TLS13 (Figures 6 and 7). Both metabolic measurements did not correlate significantly with any other sediment property.

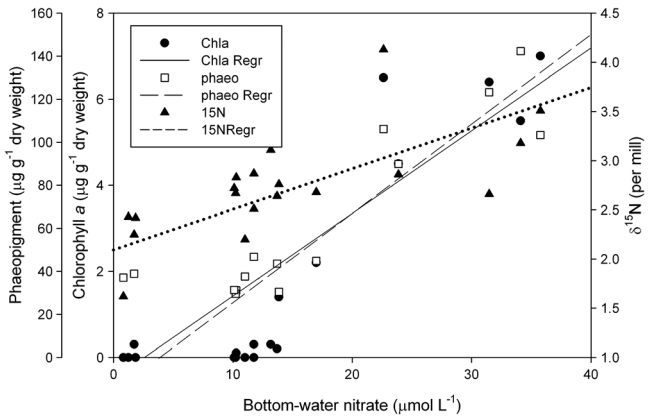

Figure 5. Surface sediment concentrations ($\mu g\ g^{-1}$) of chlorophyll *a*, phaeopigment, and $\delta^{15}N$ (‰) in relation to bottom water nitrate concentrations as a proxy indicator of upwelling. All regressions are significant ($P < 0.001$). Chla $= -0.676 + 0.162x$, $R^2 = 0.797$, $F_{1,18} = 66.682$; phaeopigment $= -1.510 + 0.286x$, $R^2 = 0.717$, $F_{1,18} = 43.049$; $^{15}\delta\ N = 2.179 + 0.048x$, $R^2 = 0.516$, $F_{1,18} = 18.102$.

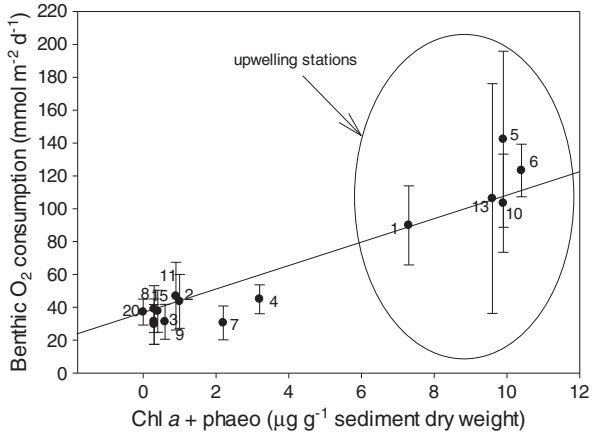

Figure 6. Rates of benthic oxygen consumption (mmol m^{-2} day^{-1}) versus total pigment concentrations ($\mu g\ g^{-1}$) in surface sediments at each of the stations along the southern Timorese shelf. Stations are identified against each symbol. Values are mean ± 1 standard deviation. Regression: $O_2 = 29.666 + 8.732x$, $R^2 = 0.921$, $F_{1,14} = 151.602$ ($P < 0.001$).

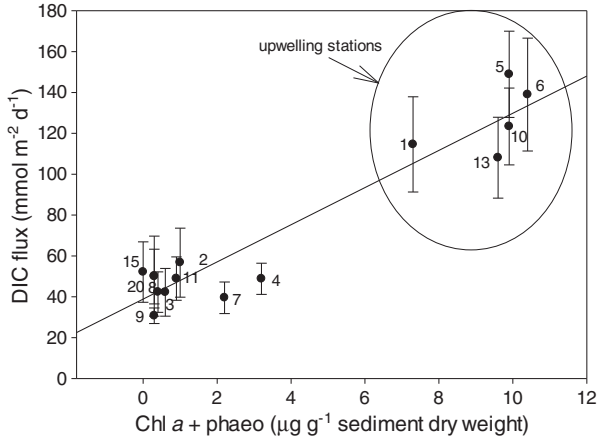

Figure 7. Rates of benthic DIC release (mmol m^{-2} day^{-1}) across the sediment-water interface versus total pigment concentrations ($\mu g\ g^{-1}$) in surface sediments at each of the stations along the southern Timorese shelf. Stations are identified against each symbol. Values are mean ± 1 standard deviation. Regression: $DIC = 38.848 + 9.103x$, $R^2 = 0.908$, $F_{1,14} = 129.025$ ($P < 0.001$).

3.4. DIC and NH_4^+ Production

[30] Rates of DIC production in incubated sediments agreed well with DIC release across the sediment-water interface, with rates ranging from 32.6 to 142.5 mmol m^{-2} day^{-1}

(Figure 8, top). Rates of NH_4^+ production mirrored DIC production rates in correlating significantly with surface concentrations of chlorophyll *a* + phaeopigment (Figure 8, top). The molar ratios of mineralized DIC:NH_4^+ correlated inversely with total pigment concentrations (Figure 8, bottom).

3.5. Rates of Sulfate, Iron, and Manganese Reduction

[31] Sulfate reduction dominated at stations toward the eastern end of the island, Stas. TLS8, TLS9, TLS15, TLS18, and TLS20 (Table 3). Sulfate reduction correlated inversely with $\delta^{15}N$ ($r = -0.713$; $P < 0.00283$) and positively with percentage terrigenous TOC ($r = +0.714$; $P < 0.0.0028$) and percentage TOC ($r = +0.673$; $P < 0.006$). Iron reduction did not correlate significantly with any other sediment property. Manganese reduction dominated anaerobic microbial metabolism at 9 of the 15 stations (Table 3), but iron reduction was dominant only at Sta. TLS11. Manganese reduction correlated with water depth

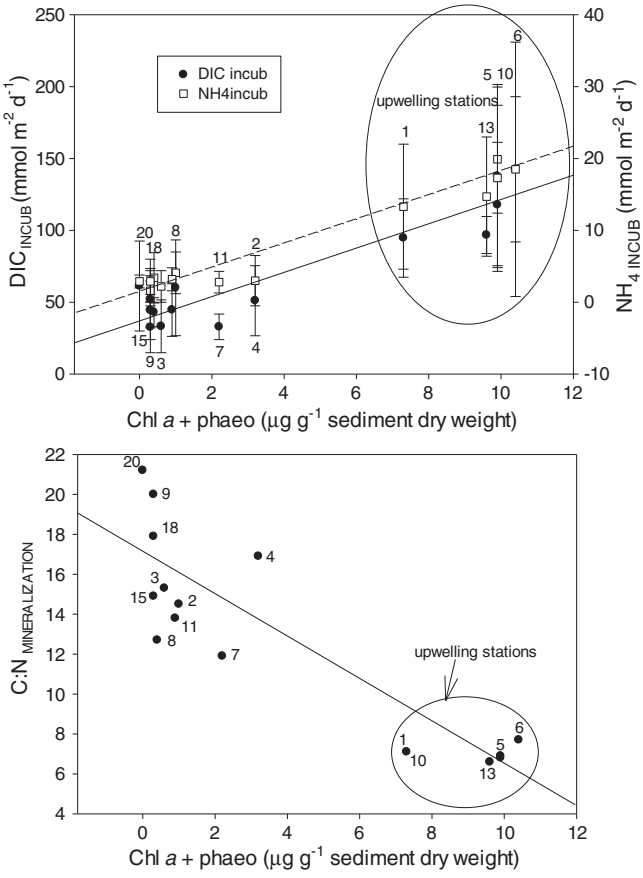

Figure 8. (top) Rates of benthic DIC and NH_4^+ production (mmol m^{-2} day^{-1}), and (bottom) molar ratios of DIC:NH_4^+ release from incubated sediments versus total pigment concentrations in surface sediments at each of the stations along the southern Timorese shelf. Stations are identified against each symbol from incubated sediments. Values are mean ± 1 standard deviation. Regressions: $DIC_{INC} = 38.561 + 8.284x$, $R^2 = 0.860$, $F_{1,14} = 79.912$; $NH_{4inc} = 1.609 + 1.575x$, $R^2 = 0.946$, $F_{1,14} = 229.637$; $C{:}N_{min} = 16.769 - 1.018x$, $R^2 = 0.763$, $F_{1,14} = 41.844$. All regressions are significant ($P < 0.001$).

Table 3. Mean (± 1 standard deviation) Rates of Sulfate (SRR), Manganese (MnR), and Iron (FeR) Reduction in Surface (0–10 cm) Sediments at Stations Along the South Timorese Coast[a]

Station	SRR	MnR	FeR
TLS1	3.8 ± 1.4 (4%)	20.2 ± 3.4 (21%)	2.1 ± 2.2 (2%)
TLS2	2.0 ± 0.4 (3%)	18.7 ± 4.0 (31%)	0.0 ± 0.0
TLS3	2.2 ± 0.6 (7%)	3.2 ± 1.8 (10%)	0.0 ± 0.0
TLS4	4.8 ± 1.4 (9%)	7.0 ± 0.0 (14%)	1.1 ± 0.8 (2%)
TLS5	2.4 ± 0.4 (2%)	25.4 ± 6.1 (18%)	1.8 ± 1.9 (1%)
TLS6	8.8 ± 2.0 (6%)	35.3 ± 2.1 (25%)	6.0 ± 4.1 (4%)
TLS7	1.8 ± 0.6 (5%)	2.2 ± 2.0 (7%)	0.0 ± 0.0
TLS8	20.4 ± 7.6 (47%)	2.4 ± 1.8 (6%)	6.1 ± 4.1 (14%)
TLS9	7.2 ± 2.0 (21%)	1.1 ± 1.4 (3%)	1.0 ± 1.0 (3%)
TLS10	1.0 ± 0.2 (<1%)	34.5 ± 3.1 (29%)	1.1 ± 2.0 (1%)
TLS11	0.6 ± 0.2 (1%)	0.0 ± 0.0	3.0 ± 3.0 (7%)
TLS13	18.4 ± 2.2 (19%)	24.6 ± 3.4 (25%)	0.0 ± 0.0
TLS14	n.d.	n.d.	n.d.
TLS15	13.2 ± 1.8 (30%)	0.0 ± 0.0	0.0 ± 0.0
TLS16	n.d.	n.d.	n.d.
TLS17	n.d.	n.d.	n.d.
TLS18	3.8 ± 0.8 (7%)	0.0 ± 0.0	0.0 ± 0.0
TLS19	n.d.	n.d.	n.d.
TLS20	37.6 ± 10.2 (61%)	0.0 ± 0.0	0.0 ± 0.0

[a]Rates are in carbon equivalents (mmol C m^{-2} day^{-1}) based on stoichiometric equations in *Alongi* [1998]. Values in parentheses are the percentage contribution of the specific pathway to TC metabolism in incubated sediments (DIC_{INCUB} in Figure 8, top panel). n.d., not detected.

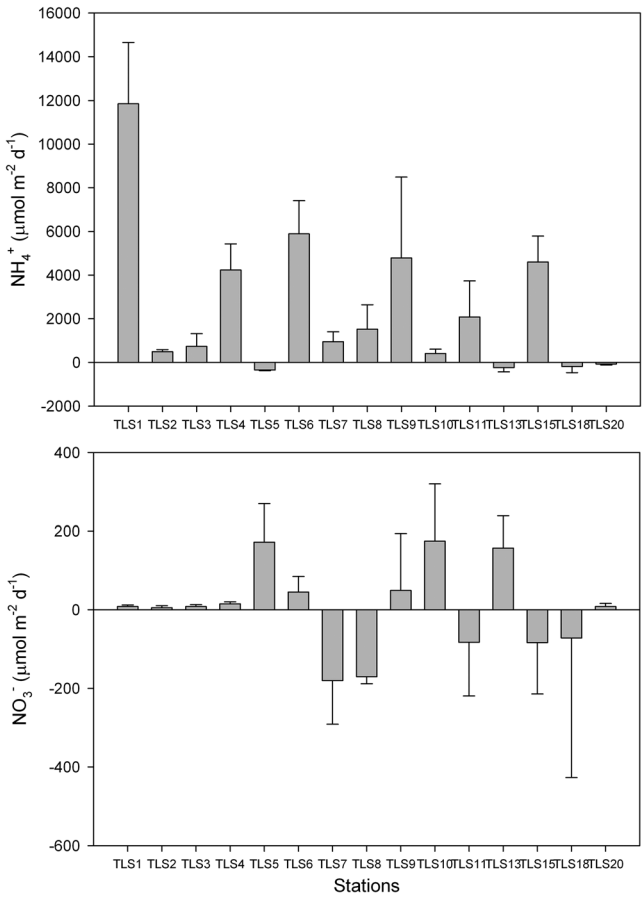

Figure 9. Rates of (top) NH_4^+ and (bottom) NO_3^- flux (µmol m^{-2} day^{-1}) across the sediment-water interface at each of the stations along the southern Timorese shelf. Values are mean ± 1 standard deviation.

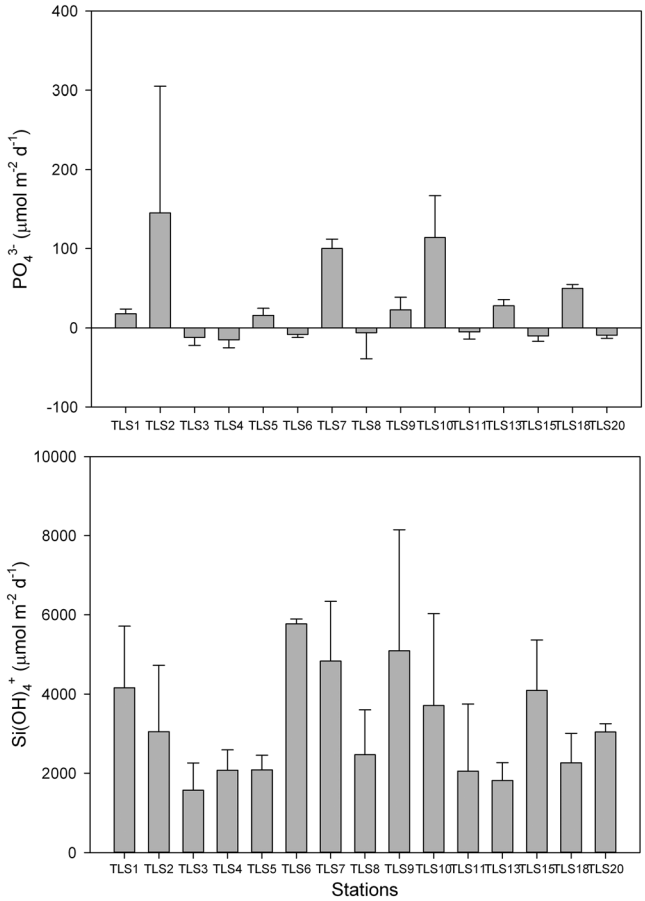

Figure 10. Rates of (top) PO_4^{3-} and (bottom) $Si(OH)_4^+$ flux (mmol m^{-2} day^{-1}) across the sediment-water interface at each of the stations along the southern Timorese shelf. Values are mean ± 1 standard deviation.

($r = +0.792$; $P < 0.0004$), $^{15}\delta$ N ($r = +0.589$; $P < 0.02$), bottom water nitrate ($r = +0.866$; $P < 0.00002$), total pigments, chlorophyll *a* and phaeopigments (r range = +0.84 to +0.93), and NO_3 flux ($r = +0.724$; $P < 0.00228$).

3.6. Nutrient Fluxes Across the Sediment-Water Interface

[32] Patterns of uptake and release of NH_4^+ (Figure 9, top), NO_3^- (Figure 9, bottom), PO_4^{3-} (Figure 10, top), and $Si(OH)_4^-$ (Figure 10, bottom) across the sediment-water interface were highly variable among stations and replicate chambers. NH_4^+, PO_4^{3-}, and $Si(OH)_4^-$ fluxes did not correlate with any variables, but NO_3^- fluxes did correlate with chlorophyll *a* ($r = +0.691$; $P < 0.0043$), phaeopigments ($r = +0.717$; $P < 0.0026$), oxygen consumption ($r = +0.728$; $P < 0.0021$), and NH_4^+ production in incubated sediments ($r = +0.716$; $P < 0.00267$).

4. Discussion

4.1. Intrusions of ITF Water

[33] Vertical water-column structure, bottom water nitrate and phosphate concentrations, and the OceanMAPS model results confirm that ITF intrusions take place along the entire southern margin of Timor, at least during the dry winter monsoon period. Most shelf waters, especially west of longitude 126°25′ (Sta. TLS13) were either highly stratified or partially stratified, with a clearly defined surface mixed layer. At the eastern end of Timor near the Timor Passage, in situ temperature profiles (Figure 2) and model results suggest upwelling of submixed layer water to the ocean surface, possibly as an eddy induced by current instabilities and strong velocity shear [*Talley et al*., 2011]. According to previous studies [*Molcard et al*., 1996; *Condie*, 2011], it is at the southeastern corner of the island that the ITF takes a more south-southwesterly direction and meets warmer surface waters sourced from the Banda Sea to the east.

[34] Along the shelf west of longitude 126°25′, the ITF intrudes as a subsurface wedge beneath lower-salinity water (Figure 2, see Sta. TLS1 profile; Figure 3, middle, section 125 E). Salinities of surface waters along the entire shelf vary little between 33.6 and 33.8, reflecting both the residual effects of river runoff during and immediately after the summer wet season, and the fact that surface waters originate from the Banda Sea. A degree of mixing and dilution is evidenced by the gradual lineal decline in dissolved nutrient concentrations from the shelf break to the nearshore zone (Figure 4). The high O_2 levels (>7 mg L^{-1}) and a salinity range of 34.3–34.6 below the top of the thermocline are consistent with the characteristics of the ITF being dominated by low-salinity, well-ventilated, upper thermocline North Pacific water [*Molcard et al*., 1996; *Sprintall*, 2009; *Schiller et al*., 2010].

[35] The vertical structure of Timorese shelf waters at other times of the year is unknown, but upwelling is likeliest to occur during the winter SE monsoon, as it does in the eastern Banda Sea [*Gieskes et al*., 1990] and along the south coasts of Java and Sumatra [*Susanto et al*., 2001]. With persistent SE trade winds blowing onshore, Ekman dynamics in the Southern Hemisphere means that shelf waters are displaced offshore in the surface layer, to be balanced by onshore flows in the lower part of the water column with an upwelling flow at the shelf-ocean boundary. Pulses of upwelling-favorable wind stress often correlate with onshore near-bed mean current flow [*Simpson and Sharples*, 2012], with concomitant declines in near-bed temperature indicating the on-shelf transfer of cooler, deeper water, and such appears to be the case along the Timorese coast. Fronts between cold, upwelled water and warmer, more dilute, shelf surface water are generally not stable [*Johnson and Rock*, 1986], with alongshore geostrophic currents on the warm side of the front generating mesoscale frontal instabilities and possible eddies. A number of small eddies, no larger than ≈ 70–100 m in diameter, were observed visually, frequently in proximity to river plumes, and these phenomena may be accentuated by strong tidal forces. Along the shelf east of longitude 126°25′, large areas of the seabed were sandy and appeared to be scoured, possibly by these onshore near-bed currents induced by wind stress and strong tides (maximum tidal range > 3 m) [*Egbert et al*., 1994].This would account for the lack of benthic enrichment along the far eastern section of the southern shelf.

[36] Intrusions of ITF water supply high concentrations of nitrate, phosphate, and silicate onto the shelf (Figure 4), whereas wind-driven offshore surface flow and other mechanisms such as eddies may export surface material off the shelf. The high concentrations of dissolved nutrients and the sharp vertical gradients in oxygen, temperature,

and salinity likely stimulated phytoplankton productivity. We were unprepared to measure primary production and chlorophyll biomass in the water column, so the chlorophyll *a* profiles measured via the calibrated fluorometer must be considered with caution and in relative terms. Our fluorescence values were exceedingly high ($>5\,mg\,m^{-3}$), greater than measured chlorophyll levels ($\leq 1.5\,mg\,m^{-3}$) within the upwelling zones off Java and Sumatra [*Susanto and Marra*, 2005], and off the northwest Australian shelf [*Furnas*, 2007; *McKinnon et al*., 2011], so they are unlikely to be correct. The high fluorescence levels likely reflect high levels of dissolved and particulate matter originating from river runoff. However, the vertical trends in fluorescence do suggest that peak plankton biomass and productivity occurred just above the 1% isolume and the thermocline at many sites (Figure 2). The comparatively high concentrations of chlorophyll and phaeopigment in surface sediments beneath the areas of subsurface upwelling offer further support for the idea of high primary productivity, as the sediment pigments must be the net result of deposition to the seabed from the overlying water column; benthic in situ production is highly unlikely given the shallow depths of the 1% light level along the shelf.

[37] Surface upwelling off the eastern end of Timor-Leste does not seem to have enhanced concentrations of nitrate, phosphate, and chlorophyll inshore at Stas. TLS19 and TLS20 (Figures 4 and 5). The CTD casts at these sites suggest that upwelling at the island's edge did not intrude close inshore, or at least may have been well mixed and diluted by strong surface flow of warmer water. The OceanMAPs results cannot be used to support the CTD data that upwelling occurs right up to the coast because model resolution was too coarse (10 km) to accurately delimit spatial patterns so close inshore.

[38] The Timor situation is analogous to the pattern of upwelling along the west coast of New Caledonia [*Hénin and Cresswell*, 2005] where coastal upwelling follows strong trade wind episodes that develop mostly in summer as a band of cold water offshore of the barrier reef; upwelling is the dominant process at daily time scales, and sea surface temperature is strongly influenced by seasonal variations in subsurface stratification [*Alory et al*., 2006]. The biological response to upwelling events is localized enhancement of offshore plankton activity followed by calm periods when there is a noticeable relaxation of plankton growth and production [*Ganachaud et al*., 2010].

4.2. Benthic Response

[39] The distribution of fine sediments on the shelf delineates the long-term net deposition of silt and clay-sized particles derived from both marine and terrestrial sources. Most deposits of smallest grain size on the Timorese shelf are located west of longitude 126°25′, reflecting the preponderance of rivers, steep catchments, and higher rainfall mid-island compared to the eastern end of the island. The sediment $^{15}\delta$ N values related positively to concentrations of dissolved nutrients in bottom waters and to both chlorophyll *a* and phaeopigment concentrations, suggesting enrichment of surface sediments in relation to enhanced primary producers associated with upwelling.

[40] The $^{13}\delta$ C values suggest a more complex picture, with the percentage of terrestrial organic carbon (Table 2) varying from a maximum of 100% off the Motaarapomaco River (Sta. TLS20) where we found extensive patches of litter derived mostly from *Lontar* palm overlying sand deposits to a minimum of 22% at one of the western stations (Sta. TLS13). Some sites (e.g., Stas. TLS7 and TLS11) also have sedimentary organic carbon that is mostly marine derived, reflecting the fact that complex distribution and transport processes must operate on this shelf. Nevertheless, on average, the western areas of subsurface upwelling had proportionally more marine-derived organic carbon (63%) than the stations (40%) further east of longitude 126°25′.

[41] Benthic metabolism was greatly enhanced beneath the subsurface intrusions of the ITF. Rates of oxygen consumption and DIC release across the sediment-water interface, and rates of DIC and ammonium production within incubated sediments correlated significantly with benthic concentrations of chlorophyll *a* and phaeopigment. Benthic metabolic activities were clearly stimulated by the deposition of phytodetritus and fresh plankton debris as a direct result of phytoplankton production enhanced by upwelling of nutrient-rich water at depth [*Asanuma et al*., 2003]. Benthic communities, especially microbial assemblages, have long been known to be enriched by rapid inputs of high-quality organic matter [*Hanson et al*., 1981]. This scenario is identical to close benthic-pelagic coupling observed in other coastal upwelling ecosystems [*Thiel*, 1978; *Barber and Smith*, 1981]. What is unusual in the Timor shelf upwelling zones are the very high rates of benthic metabolism. These rates are among the highest recorded from marine sediments [*Middelburg et al*., 2005], including from other tropical shelves where rates of oxygen consumption are usually less than $50\,mmol\,m^{-2}\,day^{-1}$ [*Alongi*, 1995, *Alongi et al*., 2007; *Aller et al*., 1996, 2008]. They are also unusually high considering the relatively low bottom water temperatures and the low (<1%) sediment organic carbon content on this shelf.

[42] The sediments (Sta. TLS20) with the highest (2%) TOC content due to significant outwelling of vascular plant detritus did not have especially rapid rates of metabolism (Figures 5 and 6) despite strong evidence of surface upwelling further offshore. As noted earlier, strong currents were observed in the region, possibly leading to scouring of the seabed rather than deposition of phytodetritus. The lower rates of benthic metabolism can also be explained by the fact that the palm tree debris observed at this site consisted of highly refractory organic matter, especially in comparison with plankton detritus, which is a more easily degradable and labile form of organic matter. Experiments have consistently shown that microbial metabolism is not readily stimulated by even high supply rates of vascular plant detritus, at least not without significant microbial enrichment and degradation over time [*Hanson*, 1982; *Tenore et al*., 1982], and such appears to be the case at Sta. TLS20. A similar scenario exists in the Georgia Bight along the southeastern U.S. coast where the inner shelf experiences significant estuarine outwelling of salt marsh detritus, whereas the outer shelf and its phytoplankton communities are greatly stimulated by intrusions from the adjacent Gulf Stream. The pattern of benthic response off the south coast of Timor-Leste is similar in that rates of microbial metabolism were

significantly higher along the outer Timorese shelf. And just like the Georgia Bight, it is unlikely that high metabolic rates are sustained for long within the upwelling zones on the Timor shelf, as labile material is usually rapidly depleted within weeks of postbloom conditions.

[43] Our metabolic measurements were made only from surface sediments and very likely do not encompass the complete range of metabolic processes occurring in these shelf deposits. Measurable rates of microbial activity, especially iron reduction, have been observed to a sediment depth of at least 1 m in sediment cores taken off the Amazon and Fly rivers [*Aller et al*., 1996, 2008], within the Great Barrier Reef [*Alongi et al*., 2007], and off the rivers of southwest New Guinea [*Alongi et al*., 2012]. Thus, the true rates and pathways of microbial metabolism on the Timor shelf are likely to be considerably different from the "snapshot" measurements taken during July 2011. Nevertheless, there are some clear patterns in the relative dominance of specific bacterial pathways in surface sediments. First, manganese reduction was rapid (Table 3) compared to rates measured in other shelf sediments [*Aller*, 1994; *Thamdrup*, 2000] and were closely linked to upwelling. Second, rates of iron reduction were low; significant iron reduction probably occurs in deeper sediment layers. Third, sulfate reduction dominated TC oxidation and was the only measurable anaerobic process in shelf sediments east of longitude 126°25′; correlation analysis indicates that sulfate reduction was linked not only to percentage organic carbon content, but also to the percentage of land-derived organic matter. Finally, although we measured only surface respiration, except for Stas. TLS8 and TLS20, 56% to 94% of TC decomposition is unaccounted for by the reduction of sulfate, iron, or manganese. Presuming that denitrification and methanogenesis were minor C oxidation pathways, which is not unreasonable considering the low organic carbon and nitrogen content of these deposits, by difference, aerobic respiration must play a significant role in surface sediments. This may not be the case if metabolism in deeper sediments had been measured, but in any case, oxic respiration plays a key role in driving benthic surface metabolism.

[44] In sediments beneath other upwelling zones, a suite of redox processes may dominate [*Gallardo*, 1977; *Glud et al*., 1999; *Sumida et al*., 2005]. For instance, under the Peruvian upwelling system, sulfate reduction and sulfide oxidation are major metabolic pathways in deep water sediments [*Gallardo*, 1977]. Regardless of the dominance of a specific diagenetic pathway, it is clear that upwelling events usually lead to enhanced benthic metabolism.

[45] Beneath the areas of subsurface upwelling, manganese reduction was the dominant metabolic pathway along with aerobic respiration. Sediment and near-bottom conditions apparently favored manganese-reducing bacteria; these assemblages outcompete other anaerobic microflora such as iron-reducers [*Ehrlich and Newman*, 2009]. Neither manganese- (Mn-) nor iron-reducing activities were measured in shelf sediments east of longitude 126°25′ (Table 3) where upwelling was not observed close inshore. The study by *Aller* [1994] in Long Island Sound suggests that manganese-reducing bacteria can respond rapidly to deposition of phytodetritus, and such may be the case off Timor-Leste. Theoretically, diagenesis involving Mn can be linked to nitrate via coupled anaerobic nitrification/lithotrophic Mn reduction reactions [*Ehrlich and Newman*, 2009]. A significant correlation ($r = +0.724$) was found between Mn reduction and nitrate flux across the sediment-water interface, although this may reflect coincident, unrelated responses to the deposition and subsequent decomposition of phytopigments.

[46] Rates of sulfate reduction were low, equivalent to rates measured on other tropical shelves [*Aller et al*., 1996, 2008; *Alongi et al*., 2007, 2012], and correlated positively with concentrations of sediment TOC and the fraction of terrestrially derived OC, indicating a possible threshold of organic carbon concentration and source. Low rates of sulfate reduction in tropical sediments have been attributed to a number of factors, including frequent sediment disturbance and the predominance of highly weathered debris exported onto low-latitude shelves [*Aller et al*., 1996, 2008; *Alongi et al*., 2007, 2012]. These drivers may apply to sulfate-reducers in Timorese shelf deposits, but their low activities may reflect the fact that they are outcompeted by manganese-reducers [*Ehrlich and Newman*, 2009]. The dominance of aerobic respiration at many sites suggests conditions, such as high bottom water O_2 levels, unfavorable for the growth of sulfate-reducing bacteria. Like other tropical shelves, aerobic and suboxic diagenesis are the main pathways of organic matter decomposition off Timor-Leste.

[47] Seasonal upwelling off Timor-Leste may play an important role in supporting higher trophic levels in shelf and offshore food webs. Large, oceanic pelagic fish, such as the southern bluefin, albacore, bigeye, and yellowfin tuna, have been caught off the Timor shelf for the past 42,000 years [*O'Connor et al*., 2011]. Tuna may be attracted to enhanced plankton productivity induced by upwelling at the shelf edge, as southern bluefin tuna are in the Great Australian Bight [*Willis and Hobday*, 2007]. The south coast of Timor is a key migration route for several species of whales and dolphins, and other megafauna (e.g., turtles) are frequently observed on the shelf [*Butcher*, 2004]. In the past, sperm whales were frequently hunted off the south coast of Timor [*Beale*, 1839; *Butcher*, 2004] and in upwelling areas of the adjacent Banda Sea [*Bennett*, 1840]. Whether large migratory megafauna are associated with the Timor upwelling is problematic but cannot be ruled out.

[48] **Acknowledgments.** This study was supported by the Australian Institute of Marine Science, the Global Environment Fund, the United Nations Development Program, and the government of Indonesia. We thank Ian Poiner for providing the ship time and supporting the expedition. We thank the captain and crew of the R.V. *Solander* for their professionalism, help, and hospitality during the cruise. A. Rustam, F, Rijoly, Awaludin, M. Stowar, and A. Heyward helped with the sampling and we thank them for their assistance and congeniality. We thank S. Boyle, C. Payn, J. Wu Won, and K. MacAllister for analyzing many of the samples. We thank C. Steinberg for helping with the physical oceanographic information.

References

Aller, R. C. (1994), The sedimentary Mn cycle in Long Island Sound: Its role as intermediate oxidant and the influence of bioturbation, O_2, and C_{org} flux on diagenetic reaction balances, *J. Mar. Res.*, *52*, 259–295.

Aller, R. C., N. E. Blair, and G. J Brunskill (2008), Early diagenetic cycling, incineration, and burial of sedimentary organic carbon in the central Gulf of Papua, *J. Geophys. Res.*, *113*, F01S09, doi:10.1029/2006JF000689.

Aller, R. C., N. E. Blair, Q. Xia, and P. D. Rude (1996), Remineralization rates, recycling and storage of carbon in Amazon shelf sediments, *Cont. Shelf Res.*, *16*, 753–786.

Alongi, D. M. (1995), Decomposition and recycling of organic matter in muds of the Gulf of Papua, northern Coral Sea, *Cont. Shelf Res.*, *15*, 1319–1337.

Alongi, D. M. (1998), Coastal Ecosystem Processes, CRC Press, Boca Raton, Fla.

Alongi, D. M., L. A. Trott, and J. Pfitzner (2007), Deposition, mineralization, and storage of carbon and nitrogen in sediments of the far northern and northern Great Barrier Reef shelf, *Cont. Shelf Res.*, *27*, 2595–2622, doi:10.1016/j.csr.2007.07.002.

Alongi, D. M., S. Wirasantosa, T. Wagey, and L. A. Trott (2012), Early diagenetic processes in relation to river discharge and coastal upwelling in the Aru Sea, Indonesia. *Mar. Chem.*, *140–141*, 10–23, doi:10.1016/j.marchem.2012.06.002.

Alory, G., A. Vega, A. Ganachaud, and M. Despinoy (2006), Influence of upwelling, subsurface stratification, and heat fluxes on coastal sea surface temperature off southwestern New Caledonia, *J. Geophys. Res.*, *111*, C07023, doi:10.1029/2005JC003401.

Asanuma, I., K. Matsumoto, H. Okano, T. Kawano, N. Hendiarti, and S. Sachoemar (2003), Spatial distribution of phytoplankton along the Sunda Islands: The monsoon anomaly in 1998, *J. Geophys. Res.*, *108*, 3202, doi:10.1029/1999JG000139.

Atmadipoera, A., R. Molcard, G. Madec, S. Wijffels, J. Sprintall, A. Koch-Larrouy, I. Jaya, and A. Supagat (2009), Characteristics and variability of the Indonesian throughflow water at the Outflow Straits. *Deep-Sea Res.*, *56*, 1942–1954.

Barber, R. T., and R. L. Smith (1981), Coastal upwelling ecosystems, in Analysis of Marine Ecosystems, edited by A. R. Longhurst, pp. 31–68, Academic Press, New York.

Beale, T. (1839), The Natural History of the Sperm Whale, J. Van Voorst, London.

Bennett, F. D. (1840), Narrative of a Whaling Voyage Round the Globe from the Year 1833 to 1836, Richard Bentley, London.

Bran, B. and L. Luebbe (1997), Directory of Autoanalyser Methods, Bran and Luebbe GmbH, Norderstedt, Germany.

Butcher, J. G. (2004), The Closing of the Frontier: A History of the Marine Fisheries of Southeast Asia c. 1850–2000. Institute of Southeast Asian Studies, Singapore.

Canfield, D. E., B. Thamdrup, and J. W. Hansen (1993), The anaerobic degradation of organic matter in Danish coastal sediments: Iron reduction, manganese reduction, and sulphate reduction, *Geochim. Cosmochim. Acta*, *57*, 3867–3883.

Chappell, J., and H. H. Veeh (1978), Late Quaternary tectonic movements and sea-level changes at Timor and Atauro Island, *Bull. Geol. Soc. Am.*, *89*, 356–368.

Condie, S. A., (2011), Modeling seasonal circulation, upwelling and tidal mixing in the Arafura and Timor Seas, *Cont. Shelf Res.*, *31*, 1427–1436, doi:10.1016/j.csr.2011.06.005.

Cresswell, G., A. Frische, J. Peterson, and D. Quadfasel (1993), Circulation in the Timor Sea, *J. Geophys. Res.*, *98*, 14379–14389.

Durand, F. (2002), East Timor: A Country at the Crossraods of Asia and the Pacific, Silkworm Books, Chiang Mai, Thailand.

Egbert, G. D., A. F. Bennett, and M. G. G. Foreman (1994), TOPEX/POSEIDON tides estimated using a global inverse model, *J. Geophys. Res.*, *99*(C12), 24,821.

Ehrlich, H. L., and D. K. Newman (2009), Geomicrobiology, 5th ed, CRC Press, Boca Raton, Fla.

England, M. H., and F. Huang (2005), On the interannual variability of the Indonesian throughflow and its linkage with ENSO, *J. Clim.*, *18*, 1435–1444, doi:10.1175/JCLI3322.1

Folk, R. L. (1974), Petrology of Sedimentary Rocks, Hemphill, Austin, Tex.

Fossing, H. R., and B. B. Jorgensen (1989), Measurement of bacterial sulfate reduction in sediments: Evaluation of a single-step chromium reduction method, *Biogeochemistry*, *8*, 205–222.

Furnas, M. J. (2007), Intra-seasonal and inter-annual variations in phytoplankton biomass, primary production and bacterial production at North West Cape, Western Australia: Links to the 1997-1998 El Niño event, *Cont. Shelf Res.*, *27*, 958–980, doi:10.1016/j.csr.2007.01.002.

Gallardo, V. A. (1977), Large benthic microbial communities in sulphide biota under the Peru-Chile Subsurface Countercurrent, *Nature*, *268*, 331–332.

Ganachaud, A., A. Vega, M. Rodier, C. Dupouy, C. Maes, P. Marchesiello, G. Eldin, K. Ridgway, and R. Le Borgne (2010), Observed impact of upwelling events on water properties and biological activity off the southwest coast of New Caledonia, *Mar. Pollut. Bull.*, *61*, 449–464, doi:10.1016/j.marpolbul.2010.06.042.

Gieskes, W. W. C., G. W. Kraay, A. Nontji, D. Setiapermana, and A. B. Sutomo (1990), Monsoonal differences in primary production in the eastern Banda Sea (Indonesia), *Neth. J. Sea Res.*, *25*, 473–483.

Glud, R. N., J. K. Gundersen, and O. Holby (1999), Benthic in situ respiration in the upwelling area off central Chile, *Mar. Ecol. Prog. Ser.*, *186*, 9–18.

Gordon, A. L., and R. A. Fine (1996), Pathways of water between the Pacific and Indian Oceans in the Indonesian seas, *Nature*, *379*, 146–149.

Griffies, S. M., R. C. Pacanowski, and A. Rosati (2004), A Technical Guide to MOM4, GFDL Ocean Group Technical Report No. 5, 371 pp., NOAA/Geophysical Fluid Dynamics Laboratory, Princeton, N.J.

Hall, P. O. J., and R. C. Aller (1992), Rapid, small-volume flow injection analysis for $\sum CO_2$ and NH_4^+ in marine and freshwaters, *Limnol. Oceanogr.*, *37*, 1113–1118.

Hanson, R. B. (1982), Organic nitrogen and caloric content of detritus. II. Microbial activity and biomass, *Estuar. Coast. Shelf Sci.*, *14*, 325–336.

Hanson, R. B., K. R. Tenore, S. Bishop, C. Chamberlain, M. M. Pamatmat, and J. H. Tietjen (1981), Benthic enrichment in the Georgia Bight related to Gulf Stream intrusions and estuarine outwelling, *J. Mar. Res.*, *39*, 417–441.

Harris, R. A. (1991), Temporal distribution of strain in the Active Banda Orogen: A reconciliation of rival hypotheses, *J. Southeast Asian Earth Sci.*, *6*, 373–386.

Hénin, C., and G. R. Cresswell (2005), Upwelling along the western barrier reef of New Caledonia, *Mar. Freshw. Res.*, *56*, 1005–1010, doi:10.1071/MF04266.

Holbourn, A., W. Kuhnt, H. Kawamura, Z. Jian, P. Grootes, H. Erlenkeuser, and J. Xu, (2005), Orbitally paced paleoproductivity variations in the Timor Sea and Indonesian Throughflow variability during the last 460 kys, *Paleoceanography*, *20*, PA3002, doi:10.1029/2004PA001094.

Johnson, J. A., and N. Rock (1986), Shelf break circulation processes, in Baroclinic Processes on Continental Shelves, Coastal and Estuarine Series, Vol. 3, edited by C. N. K. Mooers, pp. 33–62, AGU, Washington, D. C.

Lorenzen, C. J. (1967), Determination of chlorophyll and phaeopigments: Spectrophotometric equations, *Limnol. Oceanogr.*, *12*, 343–346.

Lovley, D. R., and E. J. P. Phillips (1987), Rapid assay for microbially reducible ferric iron in aquatic sediments, *Appl. Environ. Microbiol.*, *53*, 1536–1540.

Lucas, R., and E. Lindstrom (1991), The mixed layer of the Western Equatorial Pacific Ocean, *J. Geophys. Res.*, *96*, 3343–3358.

McKinnon, A. D., J. H. Carleton, and S. Duggan, (2011), Determinants of pelagic metabolism in the Timor Sea during the inter-monsoon period, *Mar. Freshw. Res.*, *62*, 130–140, doi:10.1071/MF10170,

Middelburg, J. J., C. M. Duarte, and J.-P. Gattuso (2005), Respiration in coastal benthic communities, in Respiration in Aquatic Ecosystems, edited by P. A. del Giorgio and P. J. Le B. Williams, pp. 206–224, Oxford University Press, Oxford, U.K.

Milliman, J. D., K. L. Farnsworth, and C. S. Albertin, (1999), Flux and fate of fluvial sediments leaving large islands in the East Indies, *J. Sea Res.*, *41*, 97–107.

Molcard, R., M. Fieux, and A. G. Ilahude (1996), The Indo-Pacific throughflow in the Timor Passage, *J. Geophys. Res.*, *101*, 12411–12420.

Müller, A., and B. N. Opdyke (2000), Glacial-interglacial changes in nutrient utilization and paleoproductivity in the Indonesian Throughflow sensitive Timor Trough, easternmost Indian Ocean, *Paleoceanography*, *15*, 85–94.

O'Connor, S., R. Ono, and C. Clarkson (2011), Pelagic fishing at 42,000 years before the present and the maritime skills of modern humans, *Science*, *334*, 1117–1121, doi:10.1126/science.1207703.

Paul, D., G. Skrzypek, and I. Forizs (2007), Normalization of measured stable isotope composition to isotope reference scale—a review, *Rapid Comm. Mass Spect.*, *21*, 3006–3014, doi:10.1002/rcm.3185

Richardson, A. N., and D. J. Blundell (1996), Continental collision in the Banda Arc, in Tectonic Evolution of Southeast Asia, edited by R. Hall and D. Blundell, pp. 47–60, Geol. Soc. Sp. Publ. 106, London.

Ryle, V. D., H. R. Mueller, and P. Gentien, (1981), Automated Analysis of Nutrients in Tropical Seawater, Monograph OS-81-4, Australian Institute of Marine Science Monograph Series, Townsville, Queensland, Australia.

Saji, N. H., B. N. Goswami, P. N. Vinayachandran, and T. Yamagata (1999), A dipole mode in the tropical Indian Ocean, *Nature*, *401*, 360–363.

Schiller, A., P. R. Oke, G. B. Brassington, M. Entel, R. Fiedler, D. A. Griffin, and J. Mansbridge (2008), Eddy-resolving ocean circulation in the Asian-Australian region inferred from an ocean reanalysis effort. *Prog. Oceanogr.*, *76*, 334–365, doi:10.1016/j.pocean.2008.01.003.

Schiller, A., S. E. Wijffels, J. Sprintall, R. Molcard, and P. R. Oke (2010), Pathways of intraseasonal variability in the Indonesian Throughflow region, *Dyn. Atm. Ocean.*, *50*, 174–200, doi:10.1016/j.dynatmoce.2010.02.003.

Simpson, J. H., and J. Sharples (2012), Introduction to the Physical and Biological Oceanography of Shelf Seas, Cambridge University Press, Cambridge, U.K.

Sprintall, J. (2009), Indonesian Throughflow, in Ocean Currents, a Derivative of Encyclopedia of Ocean Sciences, 2nd ed, edited by S. A. Thorpe, pp. 125–131, Elsevier, London.

Stookey, L. L. (1970), Ferrozine-a new spectrophotometric reagent for iron, *Anal. Chem.*, *42*, 779–781.

Sumida, P. Y. G., M. Y. Yoshinaga, A. M. Ciotti, and S. A. Gaeta (2005), Benthic response to upwelling events off the SE Brazilian coast, *Mar. Ecol. Prog. Ser.*, *291*, 35–42.

Susanto, R. D., A. L. Gordon, and Q. Zheng, (2001), Upwelling along the coasts of Java and Sumatra and its relation to ENSO, *Geophys. Res. Lett.*, *28*, 1559–1602.

Susanto, R. D., and J. Marra, (2005), Effect of the 1997/98 El Niño on chlorophyll *a* variability along the southern coasts of Java and Sumatra, *Oceanography*, *18*, 124–127.

Talley, L. D., G. L. Pickard, W. J. Emery, and J. H. Swift (2011), Descriptive Physical Oceanography, 6th ed, Elsevier, London.

Tenore, K. R., L. Cammen, S. E. G. Findlay, and N. W. Phillips (1982), Perspectives of research on detritus: Do factors controlling availability of detritus to macroconsumers depend on its source? *J. Mar. Res.*, *40*, 473–490.

Thamdrup, B. (2000), Microbial manganese and iron reduction in aquatic sediments, *Adv. Microb. Ecol.*, *16*, 41–84.

Thiel, H. (1978), Benthos in upwelling regions, in Upwelling ecosystems, edited by R. Boje and M. Tomczak, pp. 124–138, Springer-Verlag, New York.

Tillinger, D. (2011), Physical oceanography of the present day Indonesian Throughflow, in The SE Asian Gateway: History and Tectonics of the Australia-Asia Collision, edited by R. Hall, M. A. Cottam, and M. E. J. Wilson, pp. 267–281, Geological Society Sp. Publ. 355, London.

Tyson, R. V. (1997), Sedimentary Organic Matter: Organic Facies and Palynofacies, Chapman and Hall, London.

Weber, M. (1902), Introduction et Description de L'Expedition Siboga-Expeditie, E.J. Brill, Leiden.

Willis, J., and A. J. Hobday (2007), Influence of upwelling on movement of southern bluefin tuna (*Thunnus maccoyii*) in the Great Australian Bight, *Mar. Freshw. Res.*, *58*, 699–708, doi:10.1071/MF07001.

Wood, L. W. (1985), Chloroform-methanol extraction of chlorophyll *a*, *Can. J. Fish. Aquat. Sci.*, *42*, 38–43.

Xu, J., W. Kuhnt, A. Holbourn, N. Andersen, and G. Bartoli (2006), Changes in the vertical profile of the Indonesian Throughflow during Termination II: Evidence from the Timor Sea, *Paleoceanography*, *21*, PA4202, doi:10.1029/2006PA001278.